Integrated Fully Superconducting Submm Receivers

V.P. Koshelets, S.V. Shitov, A.B. Ermakov, L.V. Filippenko, P.N. Dmitriev, A.M. Baryshev[2], W. Luinge[2], and J. Mygind[3],

Institute of Radio Engineering and Electronics RAS, Moscow, Russia
[2]SRON-Groningen, Groningen, the Netherlands
[3]Department of Physics, Technical University of Denmark, Lyngby, Denmark

ABSTRACT

A concept of fully Superconducting Integrated Receiver (SIR) has been developed and experimentally tested. This single-chip submm wave receiver includes a planar antenna integrated with a SIS mixer and an internal superconducting Josephson-type Flux-Flow Oscillator (FFO). The combination of narrow linewidth and wide band tunability makes the Josephson FFO a perfect on-chip local oscillator for integrated submm wave receivers. A noise temperature (DSB) below 100 K has been achieved for an integrated receiver with the FFO operating near 500 GHz. The instantaneous bandwidth of about 15% is estimated via FTS and heterodyne measurements that meet the requirements of most practical applications. The far field antenna beam is measured as f/10 with sidelobes below - 16 dB that is suitable for coupling to a real telescope antenna. A 9-pixel imaging array receiver with each pixel containing an internally pumped receiver chip is developed and tested.

Recently a reliable technique for linewidth measurements has been developed and an autonomous FFO linewidth was measured in the frequency range from 250 to 650 GHz. The feasibility of phase locking the FFO to an external reference oscillator was demonstrated experimentally. A FFO linewidth as low as 1 Hz (determined by the resolution bandwidth of the spectrum analyzer) has been measured in the frequency range 270 - 440 GHz relative to a reference oscillator. This linewidth is far below the fundamental level given by shot and thermal noise of the free-running tunnel junction.

1. INTRODUCTION

Lightweight and compact ultra sensitive submm Superconducting Integrated Receiver (SIR) with low power consumption is very attractive for both radio-astronomical research and distant monitoring of the Earth atmosphere. The new ambitious radio-astronomy multi-dish projects (e.g. ALMA) would gain considerably by using single-chip SIRs due to their lower price and better serviceability as compared to conventional approaches. A distant study of the atmospheric pollution is possible using air- or satellite borne SIRs for detection of the spectrum lines of ozone, chlorine and other elements in the submm wave range.

A SIS mixer is presently the most sensitive detector element for a heterodyne reception in the frequency range 100 - 1000 GHz [1-6]. The SIS receivers are being used successfully in radio astronomy for observation of spectra showing the lowest noise temperature in the mm and sub-mm wave range. The noise temperature of a SIS receiver is ultimately limited only by the fundamental quantum value hf/2k. Since there are many applications lacking a compact and easily tunable submm local oscillator, the direct integration of a superconducting LO with the SIS mixer is the good chance for a serious breakthrough. In this review the latest results of SIR study that were done in tight collaboration between Space Research Organization of the Netherlands (SRON-Groningen) and Institute of Radio Engineering and Electronics (IREE-Moscow) are presented.

At the moment a Flux Flow Oscillator (FFO) based on the unidirectional flow of magnetic vortices in a long Josephson tunnel junction [7] looks most developed for integration with SIS mixer. Local oscillators based on Nb-AlO$_x$-Nb FFOs have been successfully tested from about 120 to 700 GHz (gap frequency of Nb) providing power sufficient to pump a SIS-mixer (about 1 μW at 450 GHz); both the frequency and the power of the FFO can be tuned [8, 9]. A front-end noise temperature of 85 K has been achieved at 140 GHz for a waveguide integrated receiver with FFO [10]. Recent progress on the development of quasi-optical integrated receiver with FFO [11, 12] will be presented in details in this review, here just few important points are worth to be mentioned. i) A receiver DSB noise temperature below 100 K has been achieved for SIR with the internal FFO operated over the frequency range 480 - 520 GHz [13]; it means that performance of the SIS mixer is close to the quantum limit. ii) A FFO linewidth considerably below 1 MHz has been measured near 450 GHz [14, 15]. Furthermore, recently a feasibility of phase locking the Josephson FFO to an external oscillator is demonstrated experimentally [15]. A FFO linewidth as low as 1 Hz (determined by the resolution bandwidth of the spectrum analyzer) has been measured relatively to reference oscillator in the frequency range 270 - 440 GHz. iii) A FFO can be fabricated on the base the same trilayer (and by using the same technological procedure) as a SIS mixer; the complexity of FFO circuit is much lower compare to any JJ array oscillator.

2. PROPERTIES OF THE FLUX FLOW OSCILLATORS.

The FFO is a *long* Josephson tunnel junction in which an applied dc magnetic field and a bias current drive a unidirectional flow of fluxons, each containing one magnetic flux quantum, $\Phi_0 = h/2e \approx 2 \ 10^{-15}$ Wb. Symbol h is the Planck's constant and e is the electron charge. An external coil or an integrated control line with current I_{CL} can be used to generate the dc magnetic field applied to the FFO. According to the fundamental Josephson relation the junction biased at voltage V oscillates with a frequency f =$(2\pi/\Phi_0)*$V (about 483.6 GHz/mV). The velocity and density of the fluxons and thus the power and frequency of the emitted mm-wave signal may be adjusted independently by joint action of bias current and magnetic field.

Long Josephson Nb-AlO$_x$-Nb junctions with overlap geometry are used as FFOs (see inset in figure 1). The FFO length, L, and the width, W, are about 500 μm and 3 μm, respectively. The value of the critical current density, j_c, is in the range 2 - 8 kA/cm^2 (Josephson penetration depth $\lambda_J \approx 8$ - 4 μm), which corresponds to a specific resistance, R$_n$*L*W $\approx$ 100 - 25 Ω μm^2. The values of the London penetration depth ($\lambda_L \approx 90$ nm) and the junction specific capacitance ($C_s \approx 0.08$ pF/μm^2) are assumed for the numerical calculations. An active area of FFO (i. e. tunnel barrier) is usually formed in a long window of the relatively thick insulation layer (200-350 nm, SiO$_2$) between two superconducting (Nb) films (base and counter electrodes). So-called "idle" region between the overlapping electrodes adjacent to the junction forms a transmission line in parallel to the FFO. The width of the idle region is about the junction width (W$_i \approx 3$ μm) that is limited usually by the alignment accuracy of the fabrication process. One of the electrodes of FFO is employed as a control line producing the magnetic field, B$_{appl}$, while the dc current is passing along this electrode. To characterize a FFO as an rf source, a special integrated circuit comprising a well-coupled wide-band SIS detector is used. A typical set of the current-voltage characteristics (IVCs) of the FFO (measured at different magnetic fields) is shown in figure 1. Simultaneously with recording of the FFO IVCs, pump of the integrated SIS detector were measured by IRTECON system (see below). The voltage range where the FFO delivers sufficient power to pump the integrated SIS detector is marked on the top voltage axis in figure 1. The criterion of the good pump is change of the subgap tunnel current of the SIS detector at V = 2 mV due to photon assistant tunneling, ΔI, compare to the current rise at the gap voltage Ig. The ratio ΔI/Ig more than 0.25 is realized for the FFO voltages from 550 to 1070 μV (see figure 1) that corresponds to the frequency range 270-520 GHz. Actually the frequency operation range is limited by matching circuits and SIS tuning structure rather than

FFO itself. It is possible considerably change the operation range of the integrated circuit by modifying the design of the matching elements. An implementation of the FFO based on superconductors with a higher critical temperature (higher gap voltage) results in considerable increasing of the operation frequency; recently an excitation of the resonances by Josephson radiation at frequencies up to 1.5 THz have been demonstrated [16] for NbN and NbC_xN_{1-x} tunnel junctions. It should be noted that the power and frequency of the emitted mm-wave signal may be adjusted independently, the FFO power can be precisely tuned at fixed frequency. In our experiments the power can be continuously adjusted over range of about 10 dB [12, 17].
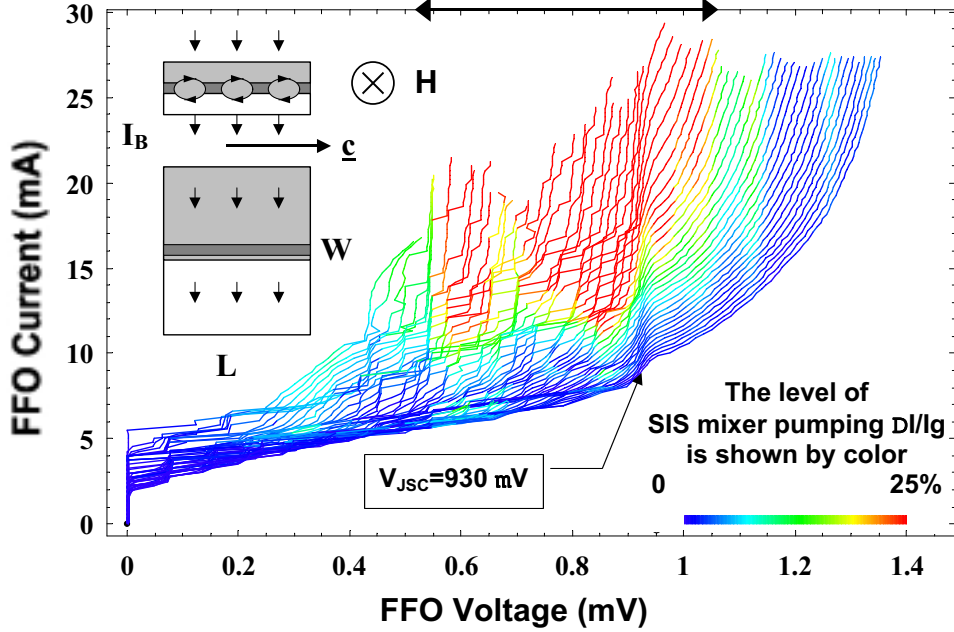

Figure 1. IVCs of the Nb-AlO$_x$-Nb FFO recorded at different magnetic fields produced by integrated control line. Note an abrupt changing of the IVC at boundary voltage $V_{JSC} \approx 930\ \mu V$. Inset presents: cross section of the long junction with driven vortices (top) and its layout (bottom). Here I_B is bias current; L and W are length and width of the FFO respectively. The level of SIS mixer pumping by FFO is shown by color.

Study of long Josephson junctions intended for wide-band integrated oscillators was performed in details [18]. Zero Field Steps (ZFSs) in the IVC of the FFO were observed for small magnetic fields. The position of the ZFS is dependent on length and propagation velocity of the electromagnetic wave along the FFO. The so-called Swihart velocity, c_{Sw}, is the maximum velocity of fluxons in the junction. The "idle" region in parallel to the junction have a much higher propagation velocity than that of the bare Josephson transmission line. This results in an increase of the effective Swihart velocity c_{Sw}^{eff} and consequently, the voltage of the ZFS, V_{ZFS}, is significantly increased. The value of c_{Sw}^{eff} depends [19] on the ratio W_i/W and, using the parameters stated above, is about $1.3\ c_{Sw}$.

The so-called Displaced Linear Slope (DLS) is observed in the IVC of the FFO at low magnetic fields. With increasing B_{appl} (see figure 1 at $V < 400\ \mu V$) the DLS branch shifts almost linearly with B_{appl} towards higher voltages. When FFO is biased within the DLS region, instead of the usual distinct superposition of quasi-particle and Shapiro steps, a "smearing" of the IVC of the SIS detector at $V \approx 0$ and $V \approx V_g$ was found [18]. It means that FFO operates as a wide-band noise source while biased at DLS. Such behavior was reported in a paper [20], where an extremely broad radiation linewidth was observed for FFO biased at the DLS. Numerical simulations [20] showed that the FFO dynamics at DLS is characterized by irregular fluxon oscillations that resemble a chaotic state. Qualitatively, the complicated fluxon dynamic can be attributed to excitation of the internal oscillation modes in the "soft" fluxon chain at weak magnetic fields.

The DLS transforms into the flux-flow step (FFS) at higher magnetic field; FFS subsequently splits [21] into a series of resonant Fiske Steps (FS) that is clearly seen in figure 1. This resonant mode takes place up to a specific "boundary" voltage, V_{JSC}, where the FSs merge into the Eck peak. At the same voltage, V_{JSC}, a "bump" in dc current appears. As also seen from figure 1 for $V > V_{JSC}$, the FFS becomes smooth and with increasing magnetic field it persists up to the gap voltage. It should be noted that this "boundary" is typical for all investigated FFO with high current density ($j_c > 1$ kA/cm^2). This feature does not depend significantly neither on the exact junction geometry and its dimensions nor on the coupling to the external microwave circuits.

The boundary voltage is about 1/3 of the superconductor gap voltage; that is ≈ 950 µV for Nb-AlO$_x$-Nb tunnel junctions. To explain the experimentally measured I-V curves, a model based on self-coupling of Josephson radiation was introduced [18]. The effect of Josephson self-coupling (JSC) [22] is basically absorption of *ac* radiation by the quasi-particles in the cavity of the long junction. It is very much related to the well-known phenomenon of photon assisted tunneling. The JSC results in current bumps (similar to quasi-particle steps in a SIS mixer) at $V_{JSC} = V_g/(2n + 1)$, which gives $V_{JSC} = V_g/3$ for n = 1. The effect of self-pumping explains not only the current bumps observed in the FFO I-V curve, but also the abrupt merge of Fiske steps (absence of resonant mode at $V \geq V_g/3$). That is caused by increase of the internal damping in the long junction due to quasi-particle tunneling [18]. In other words, the geometric resonances (or FSs) may exist only for low normalized damping, $\alpha l < 1$ (where $l = L/\lambda_J$ is the junction length normalized to the Josephson penetration length λ_J). It worth to note that the resonant conditions can be satisfied even for a very long junction, $l = L/\lambda_J \geq 100$, if the damping is sufficiently low (say, $\alpha \leq 0.01$). According to theory, the FSs transforms into so-called Eck peak when the normalized damping increases to a value of about $\alpha l \geq 2$. This threshold depends on both length and initial dumping. In accordance to qualitative calculations [18] the dumping parameter becomes five times as large for $V > V_{JSC}$ V and a FFO enters the "real" flux-flow regime with possibility of permanent frequency tuning by magnetic field.

3. INTEGRATED RECEIVER

Layout of chip receiver and experimental setup.

The submm integrated receivers [11, 13, 23, 24] are fabricated from Nb/AlO$_x$/Nb trilayer ($j_c \approx 5$ kA/cm^2) [25] on a two-inch silicon wafer (0.5 mm thick) and then diced into chips of 4 mm × 4 mm. A double-dipole antenna SIS mixer [26] is placed in the geometrical center of the chip where the incoming *rf* signal is focused by a coated silicon microwave lens [27, 28]. The FFO-based local oscillator (LO) is placed just outside the two-wavelength "hot" spot of the antenna and connected to the mixer with a microstrip transmission line, which contains a number of rf coupling and dc blocking elements. Both the SIS mixer and FFO are provided with local magnetic fields via integrated control lines [11]. All receiver elements are placed in the in the area of about 1 mm × 1 mm, but the chip dimensions are defined mainly by a size of contact pads which were chosen to be of about 0.8 mm for easier connection; eleven contact pads are provided for bond-wiring. The photograph of the receiver chip is shown in figure 2 [24].

Concept of a single-junction double-dipole antenna SIS mixer was chosen [26]. This kind of a planar integrated lens antenna is compact, although it has to use a back reflector to achieve the beam of good symmetry. The reflector is a quarter-wave thick silicon chip (800 µm × 800 µm) one-side covered with a film of Nb. The double-dipole antenna against the back reflector is treated as a four-dipole array immersed into a silicon medium ($\varepsilon_r = 11.7$). Because of homogeneity of the medium surrounding the antennas, analytical formulas for a thick wire dipole antenna are used to estimate main properties of the real device (e.g. feed-point impedance and beam shape). The beam inside the silicon media was estimated taking into account the mutual interference of all four antennas [29].
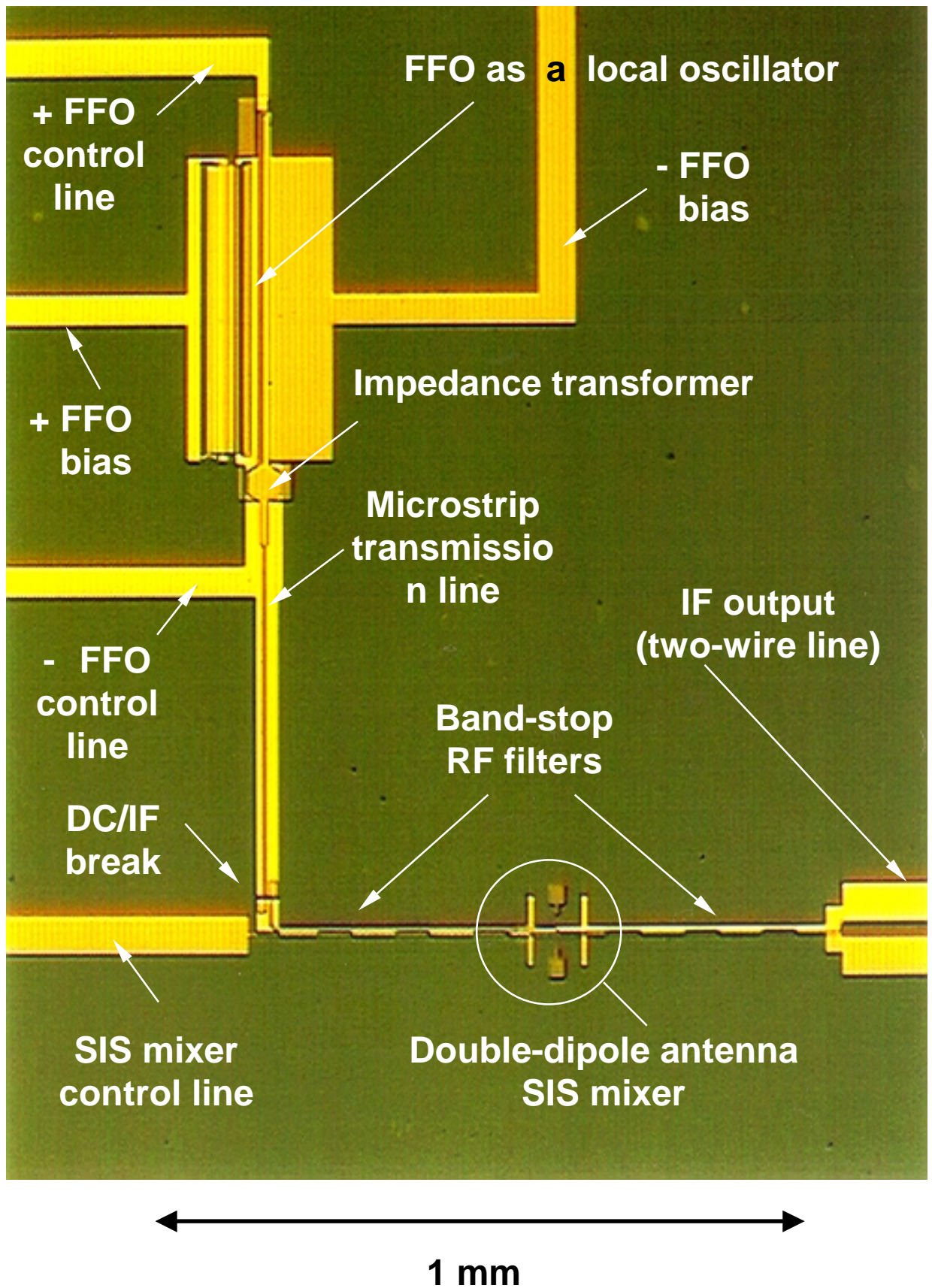
Figure 2. Microphotograph of a central part of the silicon chip of sizes 4 mm by 4 mm. All main elements of the Integrated Receiver are presented; the back reflector is not yet installed on the double-dipole antenna. Some details of wiring and contact pads are out of the field of view, which is about 1 mm by 1.5 mm.

The mixing SIS junction (about $1.5\ \mu m^2$ area) is placed in the center of the antenna array and connected to both antennas with microstrip transmission lines as a shared load. To improve rf coupling and achieve low-noise performance of the mixer, the capacitance of the tunnel SIS junction is tuned out within a certain frequency range around 500 GHz. Each microstrip feeder, connecting the junction to the antenna, is employed as a microstrip tuner for the half-junction while the antenna is tuned with an additional open-end microstrip stub. To supply a localized magnetic field to the SIS junction, the microstrip feeders are used in series forming a common control line. Since a narrower strip can, for a given current, produce stronger magnetic field, the width of $3\ \mu m$ was chosen in the vicinity of the junction. This width applies a limit for the fabrication misalignment, which is less than $1\ \mu m$.

The FFO of size $450\ \mu m \times 4\ \mu m$ is employed as a local oscillator. Since the frequency of Josephson oscillator has fundamental relation with *dc* voltage across the junction, the integrated LO has been tested for its tuneability via measuring a dependence of the FFO bias voltage on control line current while the bias current was kept constant. The experimental data obtained with the receiver showed almost linear behavior (permanent tuneability) in the flux-flow regime from about 500 GHz up to 700 GHz. To couple the power from FFO, which is basically a Josephson transmission line with an estimated characteristic impedance of about $0.4\ \Omega$ [30], to a narrow microstrip transmission line, a special impedance transformer is used. This two-stage tapered transformer was synthesized empirically as a stair-shaped microstrip. The power transmission line is a superconducting microstrip of about $900\ \mu m$ long and $4\ \mu m$ wide (characteristic impedance of about $14\ \Omega$). To bias the FFO and the SIS junction independently, a *dc*-break in both leads [31] is inserted at about half-way between the LO and the mixer (figure 2). The distant end of the LO path is shaped as a $1\ \mu m$-wide microstrip, which is a quarter-wave transformer providing the LO output impedance of about $60\ \Omega$ in parallel to the mixing junction. This value of impedance is chosen to intently limit the coupling between the mixer ($R_n \approx 20\ \Omega$) and the LO to about 20-30 % to avoid signal loss to the LO path. The power coupled from FFO to the mixer is shared between the SIS junction and antennas; the last part is lost into emission. It is important to note that the signal loss at the input of the mixer is in direct proportion with the LO coupling efficiency.

To minimize the signal loss due to the integrated LO, the concept of a balanced SIS mixer have been developed [23]. This mixer contains two SIS junctions each connected to its own antenna while the LO current applied in series to the junctions via a microstrip coupler. No leak of the equal in-phase (balanced) signal is possible to the LO path. The problem of limited LO power is not so severe for the balanced mixer in spite a twin-junction mixer has to consume at least twice more power than a single-junction mixer. The absence (or very low) coupling of the signal to the LO path allow use all 100 % of power available from FFO. The IF signal from such a mixer is obtained as a composition of two anti-phased signals from the two mixing junctions.

An elliptical silicon lens (truncated ellipsoid $R_1 = 5$ mm, $R_2 = 5.228$ mm) is designed to be the only optical element providing a diffraction limited beam f/10 at 450 - 550 GHz [27, 28]. To improve the beam coupling via reducing reflection at the interface silicon-vacuum, an antireflection coating ($87\ \mu m$ thick) made from Stycast 1264 epoxy ($\varepsilon \approx 2.9$) is applied to the lens. Both the lens and its antireflection layer have been fabricated by diamond turning with surface accuracy better than $5\ \mu m$. The chip is installed on a flat back of the lens using a paraffin wax or a soft "3M" 2216 epoxy in such a way that the antenna is, within an accuracy of $\pm 10\ \mu m$, in the focus of the lens. A printed circuit board (PCB), which provides mechanical support for *dc*- and *IF*-connections, presses the lens down against a cold (about 4.2 K) copper block installed in vacuum space of the optical cryostat with liquid helium (see figure 3).

It is worth to remind here that FFO is a magnetic sensitive device. For this reason a special shielded setup has been developed (see figure 3). The shielding inside the cryostat is provided by two coaxial cans with external layer made from cryo-perm and internal one made from copper covered with $100\ \mu m$ of superconducting led. A thermal coupler made from copper (the "leg") is

6

holding the chip far enough from the opening of the shield. The superconducting shield can be heat up to remove a trapped magnetic flux. The shield and the "leg" are thermally isolated from each other having independent heat contacts to the bottom of the liquid helium bath. To reduce risk of flux trapping in the shield, a *magnetically shielded* ferrite isolator is used at the input of the IF amplifier. The shield was tested qualitatively with a strong constant magnet (about 2000 G in the gap of 5 cm between poles) moved around at 5 cm distance from the opening of the shield (near the cryostat window). The voltage shift of about 2 μV was detected at the FFO at fixed bias current; the suppression factor of about 10^{-4} has been estimated. The cross-talk between control lines of SIS mixer and FFO was also measured and found at the level of about 10^{-3}.
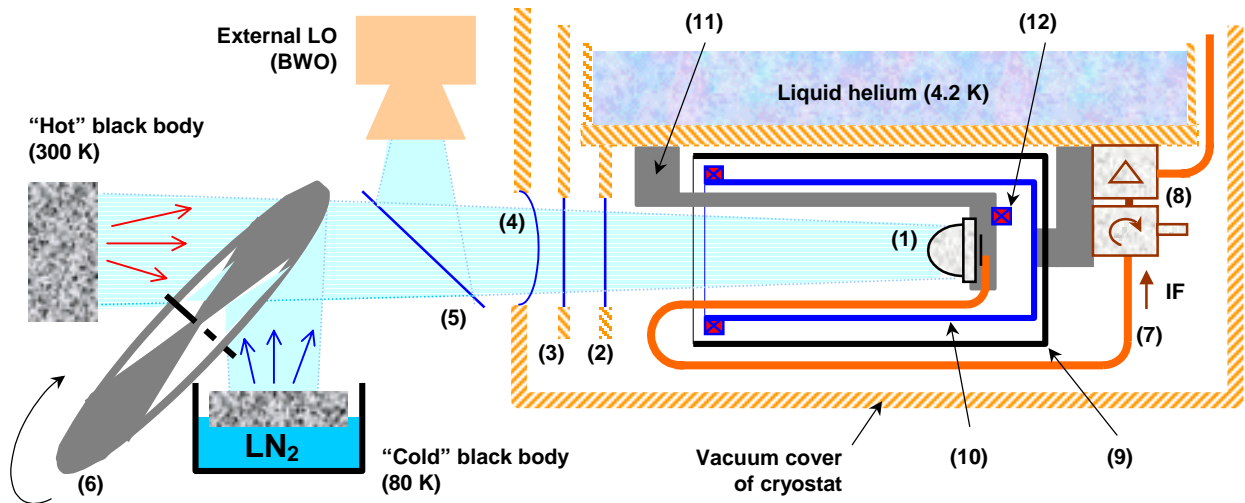

Figure 3. Schematics of experimental setup including details of beam coupling and magnetic shielding: (1) silicon elliptical lens with antireflection coating; chip receiver is glued at its flat back, (2) Zitex infrared filter at 4.2 K, (3) resonant plate filter from Teflon or quartz at 80 K, (4) resonant vacuum window from Mylar or Kapton, (5) thin film beamsplitter (not used with internal LO), (6) chopper wheel switching "hot" and "cold" antenna loads ($f_{chop} \approx 11$ Hz), (7) semirigid coaxial IF cable, (8) shielded IF isolator and 30 dB IF amplifier (1.3-1.8 GHz), (9) external shielding layer (μ-metal), (10) internal superconducting shield, (11) holder (heat sink) from copper, (12) heaters for chip and superconducting shield.

Data acquisition system IRTECON

A data acquisition system for the *I*ntegrated *R*eceiver *Te*st and *Con*trol (IRTECON) was developed for automatic collection of *dc* and *rf* data [24]. The basic system includes an analogue bias supply, designed as a standard 19" rack, and a controlling computer. The controlling computer is equipped with two acquisition cards from "National Instruments": a 16-bit resolution card for FFO and a 12-bit resolution card for the SIS mixer. Four DAC's and 10 ADC's are used in the system to hookup the analogue bias supply, the rf-detector and the lock-in amplifier. The software package is written under "LabWindows" in such a way that it can be configured for a wide range of experiments. The general view of the setup is presented in figure 4.

The IRTECON measures IV-curves of both FFO and SIS mixer and allows visualization of the pump level of the mixer in a quasi-color (see figure 1). The blue color (of the rainbow palette) on the IV-curve of FFO corresponds to the dark current of the mixer (i.e. no pump) while the red color is associated with a threshold behind which the pump (i.e. photon-induced current in the mixer) is sufficient for the optimal heterodyne reception. The size and position of the red region is a qualitative, but very convenient visual data. Setting FFO at the center of this region, one can obtain about the maximum available pump.

Figure 4. Photo of the experimental set-up controlled with IRTECON system: quasi-optical cryostat at the left, bias supply unit in the center (at the background) and data display at the right.

One of the most advanced routines is optimizing the receiver noise temperature, T_{RX}, within a particular frequency range via selection of both the optimum pump level and the best bias point for the SIS mixer. The LO power supplied to the SIS mixer is varied via FFO bias current while the LO frequency is kept constant by adjustment of magnetic field (i.e. via control current of the FFO). The Y-factor is measured at $IF \approx 1.5$ GHz with a fast *rf* detector, lock-in amplifier and running "hot/cold" chopper (see figure 3). Since the traces of T_{RX} vs. mixer bias usually are *not* crossing each other, the lowest noise figure is assumed belonging to the lowest curve. It means that optimum pump level can be found using any reasonable bias voltage, V_{SIS}, within the range of about 1-2.5 mV. At following step an optimization of the receiver noise temperature on the SIS mixer bias voltage takes place. The described routine is intended for finding and long term tracking of the (static) regime of the receiver.

Imaging Array Receiver

A focal plane Imaging Array Receiver has been designed using the fly's eye concept [13, 23, 24] whereby all 9 pixels are identical and easily exchangeable integrated receiver units described above, each with individual antireflection-coated elliptical silicon optics and individually controlled local oscillator (figure 5a). The pixels are arranged in two rows (4+5), as presented in figure 5b, using honeycomb packaging resulting in an equal distance of about 13 mm between all adjacent units. The array block was mounted on the cold plate of a specially designed cryostat equipped with a resonant Mylar window (10 cm in diameter, 180 μm thick). Because of the large window size, a number of filters are used to reduce the heat (infrared) load on the LHe vessel: a 6 mm thick plate from Teflon at 80 K and a Zitex membrane at 4.2 K stage. The shielding enclosure of the array is basically a scaled version of one described above.
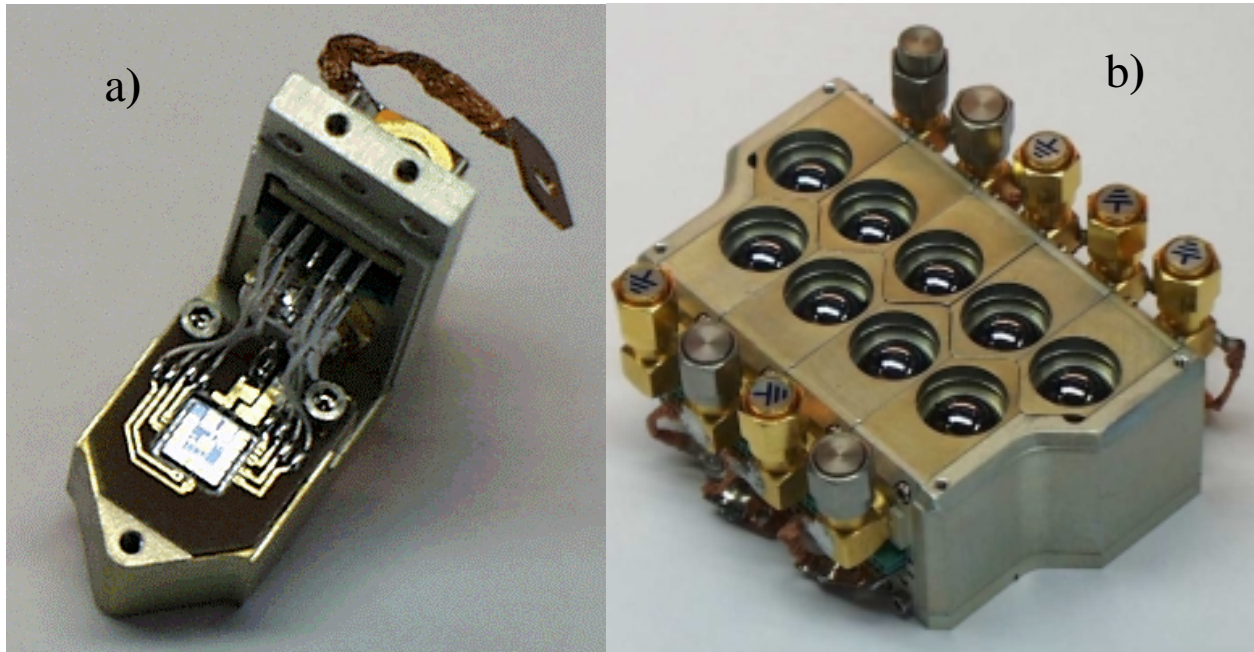
8

Figure 5. a) Replaceable element of the 9-pixel imaging array. The unit is shown from the side of the receiver chip, which is mounted on the elliptical microwave lens and wire bonded to the printed circuit board. b) Nine-pixel imaging array receiver block. Each pixel is an independent integrated receiver with its own internal local oscillator. The array mount is shown from the side of its input microwave lenses.

Only two channels were possible to monitor simultaneously during test of the array, because of deficit of both space inside cryostat and coolable IF amplifiers. A DSB noise temperature measured for the array is presented in figure 6 by circles. A 3-dB bandwidth of about 15% can be estimated with the lowest noise temperature of about 150 K, which is somewhat higher than a typical DSB noise temperature of about 120 K measured in the test cryostat. This can be certainly associated with loss in the thick (non-resonant) infrared filter at 80 K. There are, however, a few other reasons for the noise temperature increase. Since depth of the magnetic shield of the array has to be at least twice larger than the aperture of the opening, the output cable connecting the chip to the IF circulator, which is not allowed inside the shield, is about 40 cm long and introducing about 1 dB loss. It occurs also difficult to provide perfect cooling for the 50 Ω termination of the (shielded) circulator due to its design. All these restrictions and changes in the array cryostat arrangement caused the increase of the noise temperature of the IF channel and as a sequence the rise of the noise temperature of the complete receiver.

Noise temperature and antenna beam pattern

Figure 6 presents typical data on the double-side band (DSB) noise temperature obtained with internal LO for two types of the chip receiver: single-junction SIS mixer (circles) [11] and balanced SIS mixer (diamonds) [23]. Data in an array cryostat are not corrected for any additional loss associated with this arrangement. Data for balanced receiver are measured in a smaller cryostat intended for a single device test. This basic arrangement is presented in figure 3. Noise figures measured for the same devices in the test cryostat are about 10-20% lower for reasons discussed below.

On the base of noise contribution analysis [32] it became possible to reduce a receiver noise temperature below 40 K at 475 GHz for reference SIS mixer pumped by external LO. This is, to authors' knowledge, the lowest value reported within this frequency range. It worth to mention that the noise analysis for Integrated Receiver [32] do not show any considerable unknown noise

contribution. We demonstrated that an integrated receiver with the balanced mixer can operate with noise temperature less than 100 K (see figure 6) [13] that is at the level of the best SIS receivers with 'traditional' LO. The balanced mixer of present design has a bandwidth of 80 - 100 GHz (measured by FTS) that is, however, essentially wider than one of the single-junction integrated receiver (see figure 6).
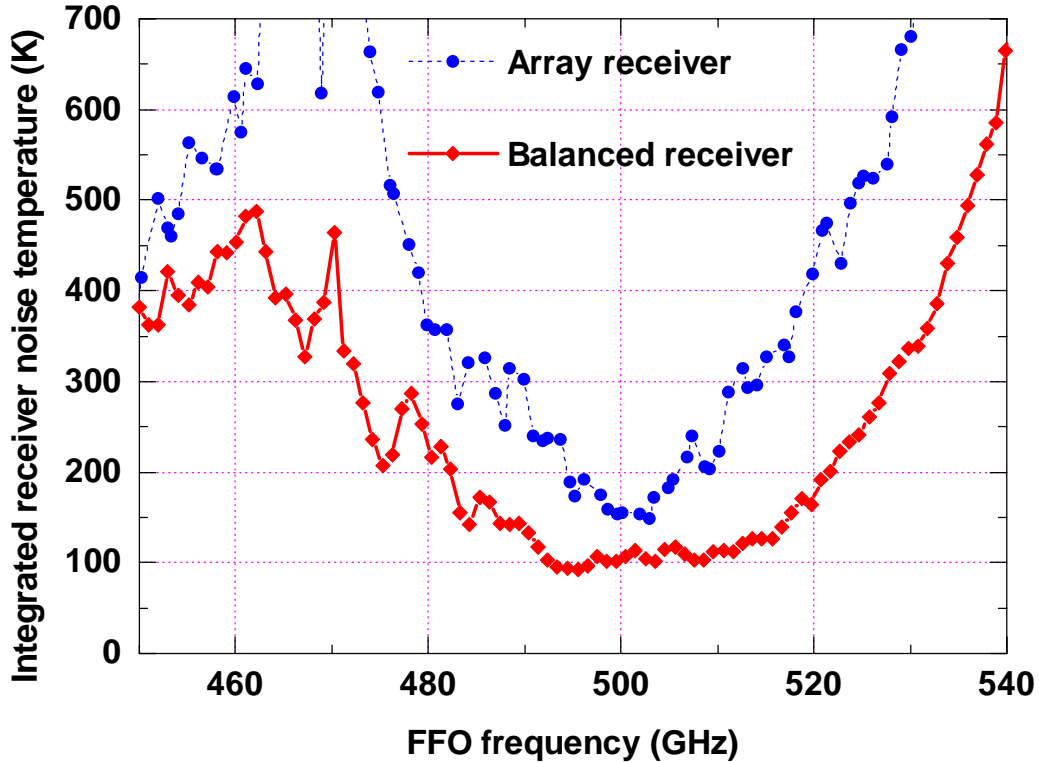

Figure 6. a) Experimental data on a typical single-junction pixel pumped by its internal FFO in 9-pixel array cryostat. The data are collected automatically by the IRTECON system; ripples are associated with interference on a thick 80 K infrared filer. b) Data on a pixel with the double-junction *balanced SIS mixer* pumped by the integrated FFO measured in smaller test cryostat.

The beam of receiving antenna is formed by a few elements: i) the printed double-dipole antenna; ii) back reflector attached to the chip and iii) the elliptical lens described above. The antenna beam pattern, presented in figure 7, was mapped in front of the window of the test dewar at the distance of 40 cm. The mapping principle is based on detection of a broad-beam source, which is being translated in front of the cryostat in the plane perpendicular to the receiver beam axis. The level of the first-order sidelobe was found at about - 16 dB with the beam width of 3.7° and 6.7° at the -3 dB and -10 dB levels respectively. The first minimum in the radiation pattern occurs at approximately 4.5°. This corresponds roughly to a f/9.4 beam with a waist size $w_0 \approx 3.6$ mm. The cross-polarization component as calculated and measured is approximately 20 dB below the co-polar level. The comparison with reference mixer showed that complex LO circuitry located in the antenna-mixer has a minor effect on the antenna beam pattern, which is in good agreement with the theoretical prediction [27, 28]. Data on antenna-beams of two neighboring pixels for Imaging Array Receiver were measured as well. Both beam patterns are, within the accuracy of the measurement, the same as measured in the qualification test. The separation of beams corresponds well to the mechanical position of pixels. No *rf* cross-talk within the array mount or cryostat has been found, unless a mirror-like obstacle is installed in front of the cryostat in a special experiment and some LO power can be directed (reflected) from one pixel to another.
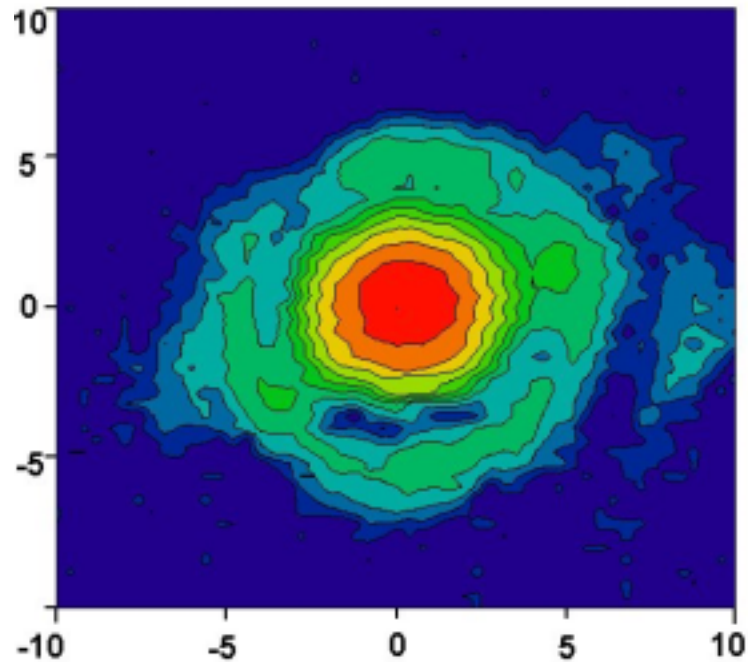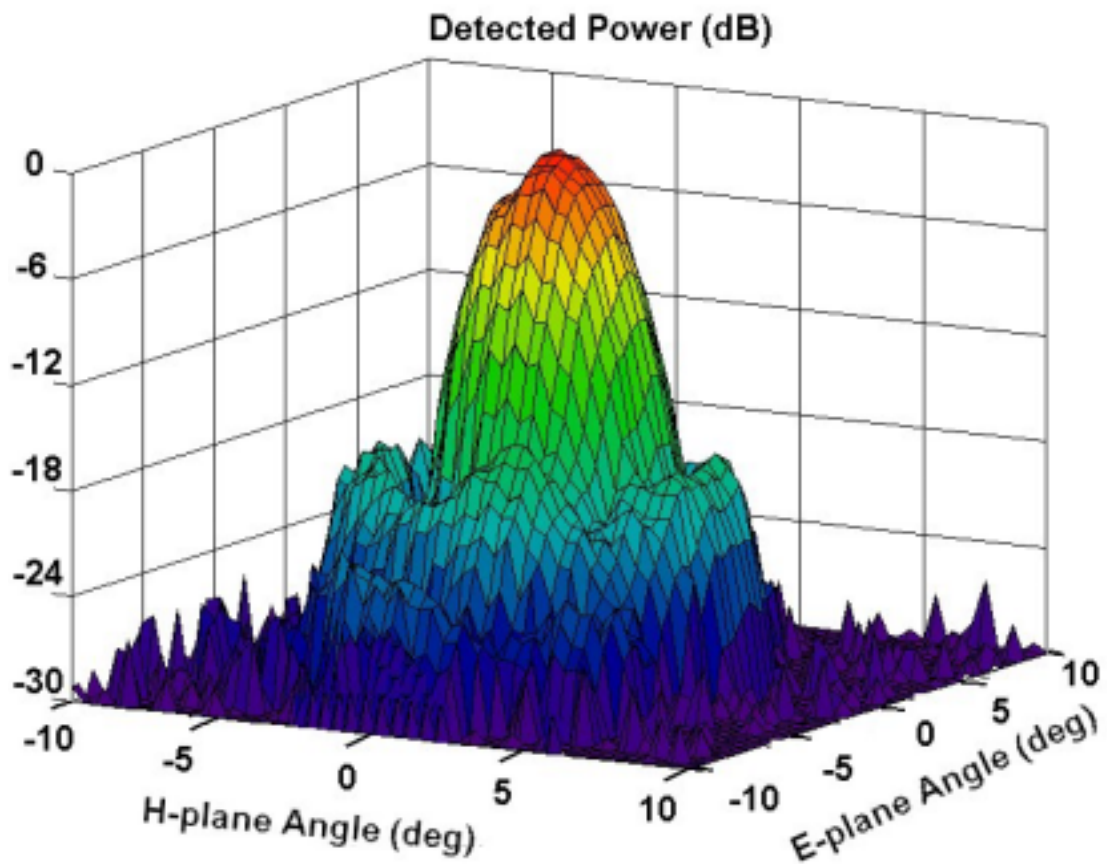
Figure 7. Antenna beam pattern of the SIR pixel measured at the distance of 400 mm from the cryostat window at 490 GHz. Data for the raster image are collected from area 100 mm by 100 mm. The equal power contours are placed with step of 1 dB. The first sidelobe found at -16 dB. Some asymmetry is assumed to be a result of sidelobes touching the shielding can.

3. FFO LINEWIDTH; PHASE LOCKING TO AN EXTERNAL OSCILLATOR.

Frequency resolution of a receiver (along with the noise temperature and the antenna beam pattern) is one of major parameters in spectral radio astronomy. The resolution is determined by both the instant linewidth of the local oscillator and its long-time stability; it should be much less than 1 ppm of the center frequency. Previous measurements on linewidth of FFO [8, 33-36] have demonstrated the following values; 130 kHz at 70 GHz [33], about 1 MHz at 280 GHz [8, 34], and 2.1 MHz at 320 GHz [35]. Recently linewidth considerably below 1 MHz have been measured near 450 GHz [14]. Unique time resolved measurements of FFO radiation were performed by using Acousto-Optical Spectrometer (AOS) with an integration time of 1 μs; the linewidth of free-running FFO less than 1 MHz at 350 GHz has been demonstrated [36]. However, the observed FFO linewidth is almost one order of magnitude wider [8, 34] than predicted by the theory for a lumped Josephson tunnel junction.

Linewidth of the FFO.

Presently no reliable theory exists for the FFO linewidth, but preliminary estimations [37] have been done on the basis of the general theory for the radiation linewidth of the *lumped* Josephson tunnel junction [38]. The linewidth, Δf, of a Josephson junction is mainly determined by low frequency current fluctuations. For white noise it can be written (see e.g. [39]) as:

$$\Delta f = (2\pi/\Phi_0^2) (R_d^B)^2 S_i(0), \tag{1}$$

where $S_i(0)$ is the density of the low frequency current fluctuations, $R_d^B = \partial V/\partial I_B$ is the dc differential resistance which transforms the current fluctuations to voltage (and phase) noise.
For a lumped tunnel junction [38, 39]

$$S_i(0) = (e/2\pi) I_B(V_{dc}) \coth(v), \quad \text{with} \quad v = (eV_{dc})/(2 k_B T_{eff}), \tag{2}$$

where k_B is Boltzmann's constant. I_B and V_{dc} are the current and averaged dc voltage in the bias point. T_{eff} is the effective temperature of the quasiparticles in the junction electrodes. This formula describes a nonlinear superposition of thermal and shot noise. It should be noted that formula does not take into account the spatial variation of the tunnel current along the FFO, the interactions of the moving fluxons, and the influence of the external low frequency interference. All these effects are believed to increase the FFO linewidth.

Fluctuations in the external magnetic field can be accounted for by the differential tuning resistance of the control line $R_d^{CL} = \partial V_{FFO}/\partial I_{CL}$ for fixed dc bias current I_B. In the case of an *external interference* both the "usual" differential resistance R_d^B and R_d^{CL} "convert" low frequency external noise currents, $I_{lf}^{(B, CL)}$, to frequency fluctuations following the same relations:

$$\Delta f \propto R_d^{(B, CL)} * I_{lf}^{(B, CL)}. \tag{3}$$

According to this theoretical consideration a radiation linewidth is determined by both the noise level and the differential resistance of the FFO at low frequencies, $f < \Delta f_{AUT}$, where Δf_{AUT} is an autonomous FFO linewidth. Since FFO is a perfect voltage-controlled oscillator, one can assume that FFO linewidth can be changed (stabilized) by an external phase-lock loop (PLL) which bandwidth is larger than Δf_{AUT}.

Experimental setup

A specially designed integrated circuit comprising the FFO, the SIS mixer, and elements for rf coupling, is used for linewidth measurements. Both the SIS and the FFO junctions are fabricated from the same Nb-AlO$_x$-Nb trilayer, details have been described elsewhere [14, 18].

The FFO linewidth was measured within wide frequency range up to 600 GHz using a new experimental technique [14]. The signal from FFO is applied to the harmonic mixer (SIS mixer operated in Josephson or quasiparticle mode) along with the signal from the frequency synthesizer f_{SYN} (about 10 GHz). To prevent the signal of the synthesizer (as well as its low harmonics) from reaching the FFO a high-pass microstrip filter with a cut-off frequency of about 200 GHz is inserted between the FFO and the harmonic mixer. The intermediate frequency (IF) signal with frequency, f_{IF} = ±(f_{FFO} – n f_{SYN}) is boosted by a cooled amplifier (T_n ≈ 20 K, gain = 27 dB gain) and then by a room temperature amplifier for further use in the PLL system. A part of the signal is applied via the directional coupler to a spectrum analyzer which is also phase locked to the synthesizer using a common reference signal at 10 MHz. This down-converted spectrum of FFO is presented in figure 8. Thus, the spectrum obtained at about 400 MHz, as well as the phase noise evaluated from these data, is a difference between the FFO signal and the n-th harmonic of the synthesizer.

In the PLL unit the IF_{PLL} ≈ 400 MHz is divided by four and compared in a Frequency-Phase Discriminator with a 100 MHz reference signal (also phase locked to the main 10 GHz synthesizer). The output signal proportional to the phase difference is returned via the Loop Bandwidth Regulator (maximum bandwidth about 10 MHz) and then feed-back to the FFO via a coaxial cable terminated with cold 50 Ω resistor mounted on the chip bias plate. To reduce the number of wires entered the cryostat, the same coaxial cable is used both for the 10 GHz synthesizer signal and for the feed-back PLL current.

In order to perform accurate linewidth measurement of free-running FFO, the IF spectra have to be averaged with a sufficiently narrow video bandwidth. The PLL system with a relatively low loop gain and narrow bandwidth setting (< 10 kHz) can be used for *frequency locking* of the FFO in order to measure an autonomous linewidth, Δf_{AUT}, of the free-running FFO. In this case it is assumed that only low-frequency noise and drifts are eliminated by the narrow-band feedback. Thus the linewidth, determined by much faster fluctuations, which assumed to be the "natural" ones, can be carefully measured.

Results and discussion

Recently the feasibility of phase locking the Josephson FFO to an external reference oscillator is demonstrated experimentally [37, 15]. It was found experimentally that the PLL system can considerably narrow the FFO linewidth if Δf_{AUT} (measured at the -3 dB level) is smaller than the PLL regulation bandwidth, B_{PLL}. Figure 8 shows typical IF power spectra of the phase locked FFO measured at f_{FFO} = 387 GHz for different settings of the spectrum analyzer. A FFO linewidth as low as 1 Hz is presented in figure 8c being limited by the resolution bandwidth of the spectrum analyzer. This experimental fact means that the FFO linewidth can be reduced below the value determined by the fundamental shot and thermal fluctuations of the free-running tunnel junction.

A consequence of the phase locking is the appearance of a vertical step (R_d^B = 0) in the dc current-voltage characteristic (IVC) of the FFO at the voltage corresponding to the frequency f_{FFO} where the FFO is locked, see Eq. (1). The position of this step is insensitive to small changes in the control line current, that means also R_d^{CL} = 0. A hold-in range of the FFO voltage as large as 1.5 μV has been experimentally measured. This corresponds to an effective PLL regulation band of about 750 MHz. It should be noted that this vertical step is not a harmonic Shapiro step. First, it is shifted from the position of possible Shapiro step by 0.8 μV that corresponds to the PLL input frequency of 400 MHz. Furthermore, the position of the vertical step was being tuned precisely by changing the reference signal. The reference signal in the range 90 - 110 MHz was applied from a second synthesizer phased locked to the first one in steps of 0.1 Hz (minimum increment of the synthesizer). This corresponds to a voltage accuracy of $2*10^{-16}$ V.
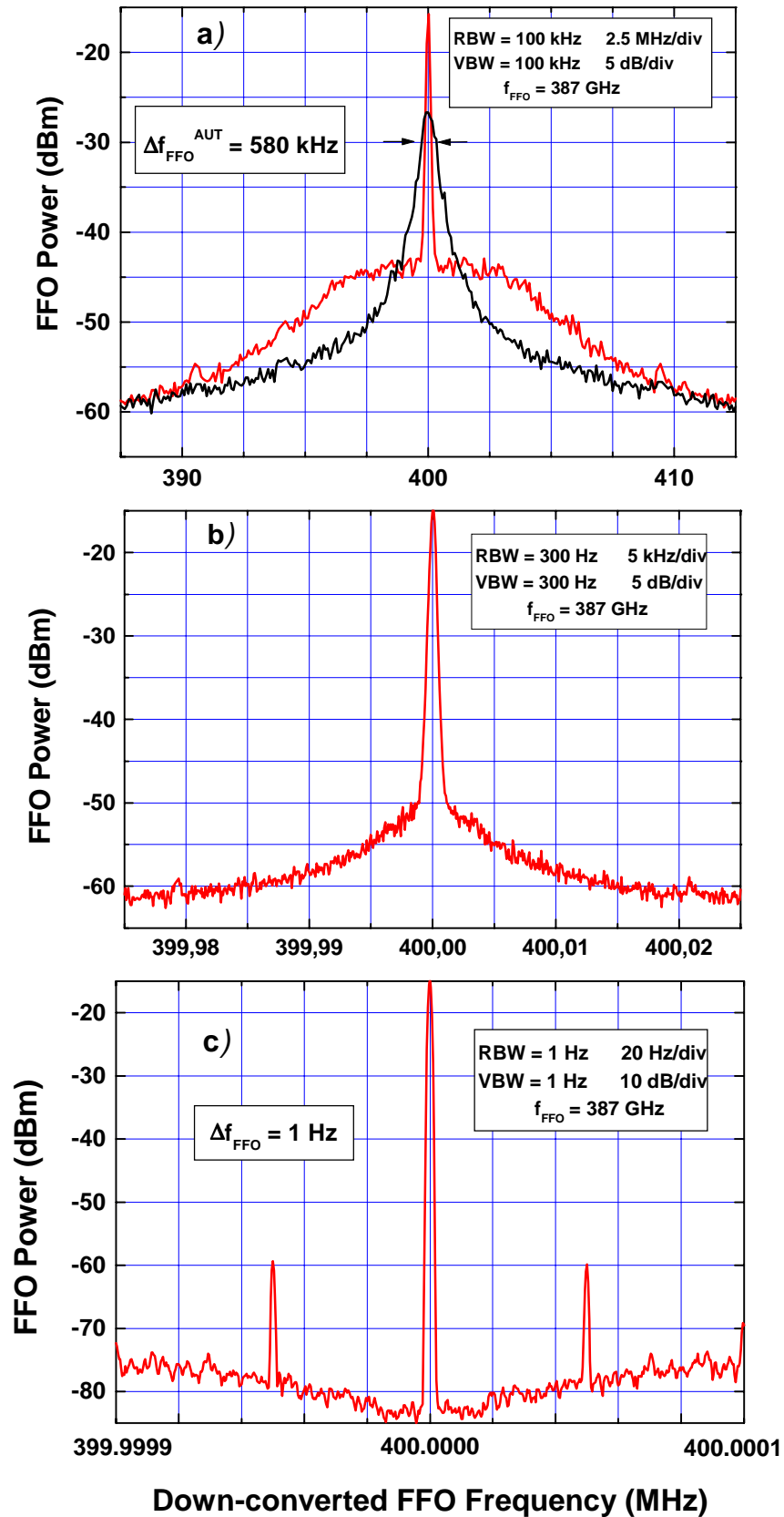
Figure 8. [15] The down-converted IF power spectra of FFO (f = 387 GHz) recorded with different frequency spans clearly demonstrates the phase locking.

14

The residual phase noise of the phase locked FFO (measured relative to the reference synthesizer) is plotted in figure 9 (data from figure 8) as function of the offset from the 400 MHz carrier. The specification and measured data for the used synthesizer (HP83752B) are shown in figure 9 as well. The FFO was locked to the 36-th harmonic of the synthesizer at this measurements, and, to get the real FFO phase noise, one should add to the measured residual FFO phase noise the synthesizer noise multiplied by $n^2 = 1296$ as shown in figure 9.

It should be noted that phase locking of the FFO has been realized only on the steep FS's, where the free-running FFO linewidth is about 1 MHz that associated with the small values of R_d^B and especially R_d^{CL}. An increase of the FFO linewidth has been found at voltages above boundary voltage, V_{JSC}, [18]; where the IVC of the FFO is modified as a result of the abrupt increase of internal damping due to Josephson self-coupling. It is still an experimental challenge to obtain phase locked operation of the FFO in the "true" flux flow regime where the normalized damping α $L/\lambda_J \geq \pi$ and initial autonomous FFO linewidth is about 10 MHz. For operation at all FFO voltages including $V > V_{JSC}$ additional efforts should be undertaken to decrease the dynamic resistance and thus the initial FFO linewidth. Also an ultra-wide-band PLL system with sufficiently low phase noise is needed. In this context the ongoing development of an on-chip integrated phase detector looks promising. The PLL bandwidth in this case will not be limited by the electrical properties of the long interconnection cables. The cryogenic phase detector, low noise amplifiers, etc. can be constructed using existing superconducting electronic components.
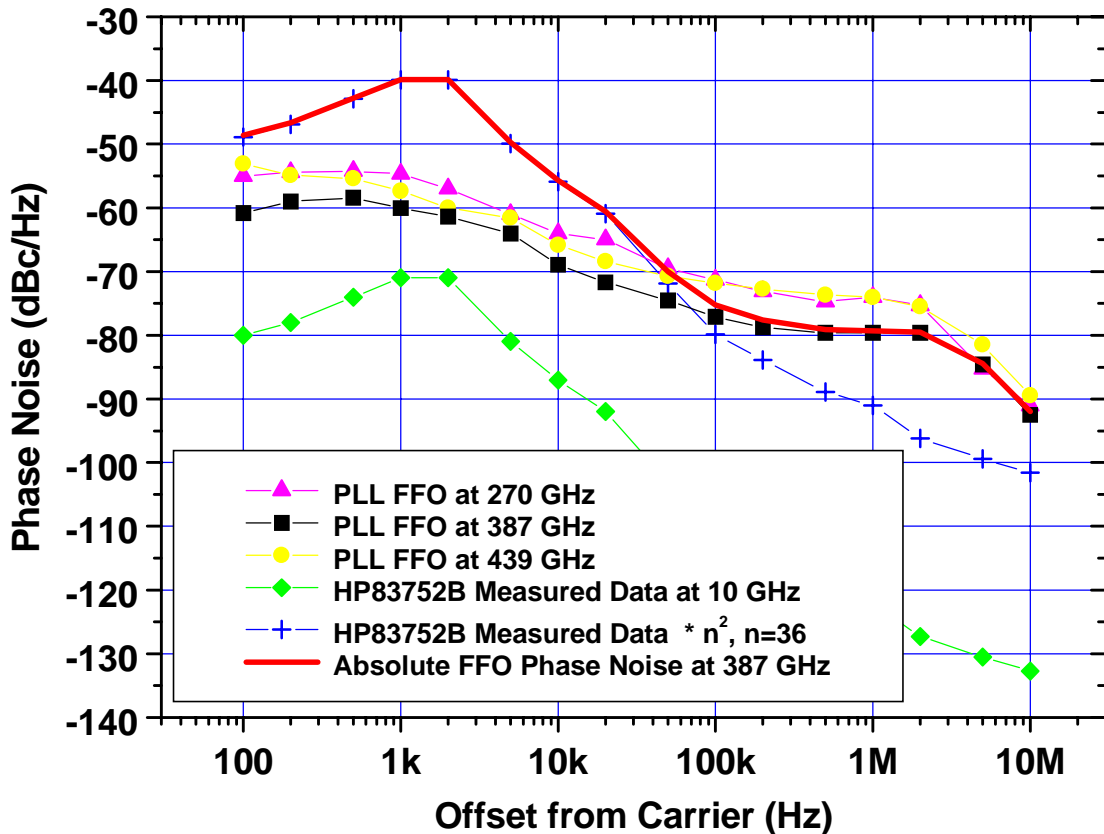

Fig. 9. Experimental phase noise of a phase locked FFO at different frequencies. Since the phase noise of the FFO, e.g., at 387 GHz is measured relative to the 36th harmonic of the synthesizer, the synthesizer noise, multiplied by a factor $36^2 = 1296$, should be added to residual FFO noise to get the total (absolute) FFO phase noise – solid line.

Recent results on phase locking of FFO to an external reference oscillator have been used to develop a concept of an integrated receiver with phase-locked loop [37, 40]. Following this concept the 350 GHz receiver chip containing a quasioptical SIS mixer, a phase-locked flux-flow oscillator, a harmonic SIS mixer and a SIS multiplier as a source for the harmonic mixer (optional) has been designed, fabricated and pre-tested recently [40, 41]. The FFO has to be phase-locked to the 35th harmonic of a 10 GHz synthesized source using custom-design room temperature electronics with PLL loop bandwidth of about 10 MHz.

Present state of development of the PLL Integrated Receiver is, so far, quite encouraging. The receiver contains well-understood devices and can be tested in the nearest future for practical spectral radio astronomy in the frequency range 350-450 GHz. In this frequency range the Fiske steps of $Nb-AlO_x-Nb$ FFO are closely spaced and almost overlapping due to finite slope and dispersion in the long Josephson tunnel junction [21]. The frequency gaps between the available LO bands (at subsequent FS's), where FFO phase locking is possible, do not exceed 5 GHz. There is a possibility to cover these gaps by a receiver by using a wide-band IF amplifier with wide enough bandwidth (2-4 GHz) while FFO is biased and locked on adjacent FS, that will result in continuous frequency coverage.

CONCLUSIONS

The combination of narrow linewidth and wide-band tuneability makes FFO a perfect on-chip local oscillator for integrated submm receiver for spectral radio astronomy and aeronomy applications. Implementation of the single-chip Superconducting Integrated Receiver (SIR) for new radio-astronomy projects based on a multi-receiver approach (e. g. ALMA) is especially advantageous due to lower price and better serviceability of the single-chip SIR as compared to conventional SIS receiver with a Gunn oscillator and multipliers. It is important to note that ultimate performance of the quasi-optical SIR is basically the same as for waveguide SIS receivers in the frequency range of 400 - 600 GHz while the wide-band tuneability and convenience of electronic control of the local oscillator (FFO) offer extra advantages of SIR over a regular SIS receiver. The data given above demonstrate electronic control of frequency and power of FFO along with the possibility of narrowing the linewidth of a Josephson oscillator using an external PLL system, provided that the PLL bandwidth is larger than the intrinsic linewidth of the free-running oscillator.

The integrated receivers fabricated on a base of niobium trilayer $Nb/AlO_x/Nb$ are proven to be useful within frequency range 100-700 GHz showing noise temperatures better than 1 K/GHz that is close to the performance of 'traditional' SIS receivers with external LO. The antenna beam properties obtained for the integrated receiver are satisfactory for use on a real telescope. A concept of the PLL integrated receiver is at the stage of intensive experimental study. The imaging array receiver based on 9 integrated receiver pixels employing elliptical silicon optics is developed and tested showing no essential degradation of the pixel performance.

References

[1] Tucker J R, Feldman M J 1985 *Rev of Mod Phys* **4** 1055-113

[2] Blondel R and Tong C E 1992 *Proc IEEE* **80** 1702-20

[3] Shitov S V, Koshelets V P, Kovtonyuk S A, Ermakov An B, Whyborn N D and Lindstrom C-O 1991 *Supercond Sci Technol* **4** 406-8

[4] Karpov A, Blondel J, Voss M, Gundlach K H 1995 *IEEE Trans on Appl Superconductivity* **5** 3304-7

[5] Zmuidzinas J and LeDuc H G 1992 *IEEE Trans on Microwave Theory and Tech* **40** 1797-804; Zmuidzinas J, Ugras N G, Miller D, Gaidis M, LeDuc H G, Stern J A 1995 *IEEE Trans on Appl Superconductivity* **5** 3053-6

[6] Gaidis M C, Leduc H G, Mei Bin, Miller D, Stern J A and Zmuidzinas J 1996 *IEEE Transactions of Microwave Theory and Techniques* **44** 1130-9

[7] Nagatsuma T, Enpuku K, Irie F, and Yoshida K 1983 *J Appl Phys* **54** 3302-9, see also Pt. II: 1984 *J Appl Phys* **56** 3284; Pt III 1985 *J Appl Phys* **58** 441; Pt IV 1988 *J App. Phys* **63** 1130

[8] Mygind J, Koshelets V P, Shchukin A V, Shitov S V and Lapytskaya I L 1995 *IEEE Trans on Appl Supercond* **5** 2951-4

[9] Koshelets V P, Shitov S V, Baryshev A M, Lapytskaya I L, Filippenko L V, van de Stadt H, Mess J, Schaeffer H and de Graauw T 1995 *IEEE Trans on Appl Supercond* **5** 3057-60

[10] Koshelets V P, Shchukin A V, Shitov S V, Filippenko L V 1993 *IEEE Trans on Appl Supercond* **3** 2524-7

[11] Koshelets V P, Shitov S V, Filippenko L V, Baryshev A M, Golstein H, de Graauw T, Luinge W, Schaeffer H and van de Stadt H 1996 *Appl Phys Lett* **68** 1273-5

[12] Koshelets V P, Shitov S V, Filippenko L V, Baryshev A M, Shchukin A V, Prokopenko G V, Litskevitch P G, de Graauw T, Luinge W, van de Stadt H, Golstein H, Schaeffer H, Klapwijk T M, Gao J-R, Lehikoinen P, Mygind J 1996 Proceedings of 30-th ESLAB Symposium *ESTEC the Netherlands* p 193-202

[13] Shitov S V, Ermakov A B, Filippenko L V, Koshelets V P, Baryshev A B, Luinge W, Gao J-R, 1999 *IEEE Trans on Appl Supercond* **9** 3773-6

[14] Koshelets V P, Shitov S V, Shchukin A V, Filippenko L V, and Mygind J 1996 *Appl Phys Lett* **69** 699-701

[15] Koshelets V P, Shitov S V, Filippenko L V, Vaks V L, Mygind J, Baryshev A B, Luinge W, Whyborn N 2000 *Rev of Sci Instr* 7**1** 289-93

[16] Kohjiro S, Shoji A 1999 presented at *EUCAS'99 Barcelona Spain* September report 6-103

[17] Koshelets V P, Shitov S V, Filippenko L V, Baryshev A B, Luinge W, Golstein H, van de Stadt H, Gao J-R, de Graauw T 1997 *IEEE Trans on Appl Supercond* **7** 3589-92

[18] Koshelets V P, Shitov S V, Shchukin A V, Filippenko L V, Mygind J, Ustinov A V 1997 *Phys Rev B* **56** 5572-7

[19] Lee G S 1991 *IEEE Trans on Appl Supercond* **3** 121-7; Thyssen N, Ustinov A V, Kohlstedt, Pagano S, Caputo J G, Flytzanis N 1995 *IEEE Trans on Appl Supercond* **5** 2965-8

[20] Ustinov A V, Kohlstedt H, and Henne P 1996 *Phys Rev Lett* **77** 3617-20

[21] Cirillo M, Gronbech-Jensen N, Samuelsen M R, Salerno M, Verona Rinati G 1998 *Phys Rev B* **58** 12377-84

[22] Hasselberg L-E, Levinsen M T, Samuelsen M R 1974 *Phys Rev B* **9** 3757-65

[23] Shitov S V, Koshelets V P, Baryshev A M, Filippenko L V, Gao J-R, Golstein H, de Graauw T, Luinge W, van de Stadt H, Whyborn N D, Lehikoinen P 1997 *Proceedings of 8th Int Symp on Space Terahertz Technology* p 281-90

[24] Shitov S V, Ermakov A B, Filippenko L V, Koshelets V P, Luinge W, Baryshev A M, Gao J-R, Lehikoinen P 1998 *Proceedings of 9th Int Symp on Space Terahertz Technology* p 263-72

[25] Dierichs M M T M, Panhuyzen R A, Honingh C E, de Boer M J and Klapwijk T M 1993 *Appl Phys Lett* **62** 774-6

[26] Skalare A, de Graauw T, and van de Stadt H 1991 *Microwave and Optical Technology Letters* **4** 9-12

[27] van der Vorst M J M, de Maagt P J I, and Herben M H A J 1996 *Proceedings of the Int Symp on Antennas (JINA '96)* p 511-5

[28] van der Vorst M J M, de Maagt P J I, and Herben M H A J 1999 *IEEE Microwave Theory and Techn* **47** 1696-705

[29] Rebeiz G M 1992 *Proceedings of the IEEE* **80** 1749-70

[30] Neman H S and Davis K L 1982 *J Appl Phys* **53** 7026

[31] Shitov S V, Koshelets V P, Shchukin A V, Baryshev A M, Lapytskaya I L, Filippenko L V, de Graauw T, Mees J, Schaeffer H, van de Stadt H 1994 *Proceedings of 19-th Int Con on Infrared and Millimeter Waves* Sendai Japan p 122-3

[32] Baryshev A B, Luinge W, Koshelets V P, Shitov S V, Klapwijk T M 1998 unpublished

[33] Ustinov A V, Doderer T, Huebener R P, Mygind J, Oboznov V A, and Pedersen N F 1993 *IEEE Trans on Appl Supercond* **3** 2287-94

[34] Koshelets V P, Shchukin A V, Lapytskaya I L, and Mygind J 1995 *Phys Rev B* **51** 6536-41

[35] Zhang Y M, Winkler D, and Claeson T 1993 Appl Phys Lett **62** 3195-7

[36] Muller U, Jacobs K 1999 *Proceedings of the 10th International Symp on Space Terahertz Techn* Clarlottesville USA p 13-28

[37] Koshelets V P, Shitov S V, Shchukin A V, Filippenko L V, Dmitriev P N, Vaks V L, Mygind J, Baryshev A B, Luinge W, Golstein H 1999 *IEEE Trans on Appl Supercond* **9** 4133-6

[38] Stephen M J 1969 *Phys Rev* **182** 531-8

[39] Likharev K K 1986 Dynamics of Josephson junctions and circuits *Gordon and Breach Science Publishers*

[40] Shitov S V, Koshelets V P, Filippenko L V, Dmitriev P N, Baryshev A M, Luinge W, Gao J-R 1999, *Proc of 10th Int Symp on Space Terahertz Techn* Clarlottesville USA p 447-58

[41] Shitov S V, Koshelets V P, Filippenko L V, Dmitriev P N, Vaks V L, Baryshev A M, Luinge W, Whyborn N D, Gao J-R 1999 *presented at EUCAS'99* Barcelona Spain report 6-100